Proceedings Australian Geothermal Energy Conferences 2013
Brisbane, Australia, 14-15 November 2013

Alteration of the Big Lake Suite granite: An answer to its enrichment in heat-producing elements

A. W. Middleton*[a], I. T. Uysal[a], S. Bryan[b], C. Hall[c] and S. D. Golding[d]

[a] Queensland Geothermal Energy Centre of Excellence, The University of Queensland, Queensland 4072, Australia

[b]Biogeoscience, Queensland University of Technology, 1 George Street, Brisbane, QLD 4001, Australia

[c]Department of Earth and Environmental Sciences, University of Michigan,

1100 N. University Ave. Ann Arbor, MI 48109-1005, USA

[d] School of Earth Science, The University of Queensland, Queensland 4072, Australia

(*correspondence: alexander.middleton@uqconnect.edu.au)

Keywords: Big Lake Suite granite, illite, Thermal and tectonic history, Warburton–Cooper Basin, ^{40}Ar–^{39}Ar geochronology, ^{87}Rb–^{87}Sr geochronology.

ABSTRACT

The Warburton–Cooper–Eromanga basins host one of the most prospective hot dry-rock geothermal resources (Big Lake Suite granite; BLS) that stems from unusual enrichment in radiogenic elements (up to 144 ppm Th and 30 ppm U). Previous studies estimate concentrations of heat-producing elements may derive from primary enrichment of minerals such as zircon. However, consequent work found unusually elevated concentrations of Th and U in areas of the granite devoid of zircon. By conducting geochemical and geochronological analyses on authigenic illite from the highly altered BLS, this study elaborates on the thermal and tectonic evolution of the region while providing an alternative hypothesis to granite enrichment.

Calculated $\delta^{18}O$ and δD fluid isotopic values of illite samples are compatible with an influx of meteoric waters in an extensional environment. Integrated geochronology (Sm–Nd, Rb–Sr, and Ar–Ar) consistently indicates the Nappamerri Trough underwent episodic tectonism at approximately 128 Ma, 95 Ma and 86 Ma. Chemically distinct periods of fluid flow are similarly inferred by distinct rare earth elements patterns for each of the age populations. Altered granite samples have substantially higher radiogenic element concentrations than the unaltered granite. Further trace element analyses also show illite samples contain unusually elevated concentrations of Th (~40 ppm) and U (~10 ppm) that contribute to ~50% of the whole-rock radiogenic element budget.

A multifaceted analytical study of authigenic illite produced geologically significant ages attributed to thermal perturbations in the Nappamerri Trough of the Warburton–Cooper–Eromanga basins. Cretaceous ages are consistent with episodic rifting of Gondwana and opening of the Tasman Sea along the eastern margin of Australia. Such consistency suggests plate-wide transmission of tensional stress to intra-continental crust weakened by abnormally high geothermal gradients, associated with the BLS, and preceding basinal tectonism. Extensional tectonism allowed an influx of evolved meteoric water that caused widespread alteration and substantial enrichment of the granite in heat-producing elements (HPE). Although the source of HPE is currently unknown, it is likely such elements were leached by moderate-temperature hydrothermal fluids from the surrounding country-rock and deposited in the granite upon illite precipitation.

1. INTRODUCTION

Rapid adjustments to intra-continental stress fields can perturb the thermal and fluid flow regimes of sedimentary basins, leading to the expulsion of basinal fluids (Kyser, 2007). During the migration of tectonically-driven fluids along permeable fracture networks, fluid–rock interaction may result in the precipitation of authigenic phases, including illite. Based on morphology and chemical composition, illite can be utilised for a number of geochemical and geochronological techniques. High magnification microscopy of illite may reveal paragenetic and morphological data pertinent to constraining fluid–rock interaction history (Reuter and Dallmeyer, 1987; Yau et al., 1987). Stable isotopic analysis of authigenic phases can also constrain fluid source, and by understanding typical variations in isotopic values, can estimate fluid evolution (Longstaffe, 2000). Trace element studies of authigenic minerals have similarly proven useful in determining physico-chemical conditions during fluid–rock interaction (Bau, 1991; Bau and Dulski, 1995; Zwingmann et al., 1999; Bau et al., 2003; Uysal and Golding, 2003; Middleton et al., under review).

The Warburton–Cooper–Eromanga basins host Australia's largest on-shore petroleum reserves. Previous work by Deighton and Hill (1998) constrained maturation and expulsion of such reserves to the "mid Cretaceous"; however, the thermal regime responsible for such expulsion is not well constrained. These basins also host one of the most prospective hot dry-rock geothermal resources in world, which stems from the presence of the abnormally radiogenic Big Lake Suite A-type granite (Hillis et al., 2004; Marshall, 2013). Early workers believed zircons to be the primary sink for HPE (K, Th and U; Wyborn pers. commun.). Chemical and microscopic analyses have since shown some highly enriched areas to be deficient of zircons, due to intense hydrothermal alteration. As such, the source and origin of the granite's radiogenic nature is still unknown. Previous tectono-stratigraphic studies of the basins identified widespread reactivated fault–fracture networks pointing towards a complex tectonic and thermal evolution that may shed light on these enigmatic resources (Apak et al., 1997; Sun, 1999; Mavromatidis, 2008). Such fracture networks would have acted as highly permeable conduits for hydrothermal fluid flow during past tectonothermal activity, that would likely

have resulted in the precipitation of authigenic clays. This in turn allows the application of radiogenic and stable isotope geochemistry to determine the timing and nature of fluid–rock interaction processes.

2. GEOLOGICAL SETTING

The stacked Warburton–Cooper–Eromanga basins extend from south-east Queensland ca. 700 km into north-west South Australia and are comprised of the early Palaeozoic Warburton Basin, unconformably overlain by the Permian-Carboniferous Cooper and Jurassic-Cretaceous Eromanga basins. At the base of the Warburton Basin are the Cambrian, bimodal Mooracoochie Volcanics, including the 'Jena' basalt, unconformably overlain by mid-upper Cambrian shales and carbonates and Ordovician siltstones and shales (Gatehouse, 1986; Meixner et al., 1999). The Warburton Basin succession is intruded by the Big Lake Suite (BLS) granite that was previously associated with the Alice Springs Orogeny (Sun, 1997) and dated at 298 ± 4 and 323 ± 5 Ma (preferred SHRIMP ages) from the Moomba 1 and McLeod 1 wells, respectively (Gatehouse et al., 1995). The BLS has two predominant cupolas that comprise the "Moomba High" that are bounded by normal faults (Apak et al., 1995).These cupolas are unusually enriched in heat-producing or radiogenic elements: K, Th and U (up to 144 ppm Th and 30 ppm U). The origin of enrichment is currently unknown, but has lead to substantial research and attempts to utilise the BLS for hot dry-rock geothermal energy (Chopra and Wyborn, 2003). The Warburton Basin is interpreted to have formed in a back-arc basin setting to the west of the Mt. Wright arc, inferring the presence of westward subduction (Roberts et al., 1990). Unconformably overlying the Warburton Basin and BLS granite are the Cooper and Eromanga basins that are arguably considered as intra-continental, sag basins (Apak et al., 1997; Cook et al., 2013).

The Gidgealpa–Merrimelia–Innamincka (GMI) Ridge is the most prominent NE–SW trending anticlinal thrust structure that is interpreted as Late Carboniferous, and divides the Patchawarra and Nappamerri synclinal troughs of the Cooper Basin (Sun, 1997; and references therein). The Cooper Basin developed structurally by the reactivation of previous faults until a period of tectonic quiescence. During this time, fluviatile, lacustrine and coal-bearing sequences were deposited until the mid Triassic (Apak et al., 1997; Mavromatidis, 2006). Sedimentation then ceased due to northeast-southwest apparent compression, resulting in basin-wide exhumation and emplacement of the Nappamerri Unconformity (Thornton, 1979; Kuang, 1985). Subsequent subsidence and sedimentation of the Eromanga Basin deposited near uniform Jurassic to Cretaceous fluvial-lacustrine and shallow marine sediments until exhumation at the Upper Cretaceous–Palaeogene boundary. The following 90 Myr are characterised by minimal sedimentation and multiple periods of exhumation (Mavromatidis, 2006; Mavromatidis, 2008).

3. SAMPLING AND ANALTICAL PROCEDURES

3.1. Sampling

Authigenic illite–smectite samples were collected from multiple drill holes within the Nappamerri Trough. 20 samples were taken from Warburton and Cooper sediments and the Big Lake Suite granite of the Nappamerri Trough (Moomba 1, 2, 7 and 72, Big Lake 1 and 57 and McLeod 1). As samples are taken from Warburton and Cooper Basin stratigraphy, they will be collectively referred to as Nappamerri Trough or GMI Ridge samples throughout the paper. If referring to an entire drill hole of samples, only the drill hole name (with no specific depth) will be given, for example MB_72 for Moomba 72 or BL_1 for Big Lake 1.

3.2. Microscopy and X-ray diffraction

Thin section studies on whole-rock samples utilised a combination of plane–cross-polarised light, scanning electron microscopy with energy dispersive X-ray spectroscopy (SEM–EDS) and transmission electron microscopy (TEM). SEM–EDS analysis used the JEOL JXA-8500F (Hyperprobe) at the Deutsches GeoForschungsZentrum (GFZ) in Potsdam, Germany. TEM examination was made with the JEOL 2100 TEM at The University of Queensland on nearly pure illite separates from GMI Ridge (sediments) and Nappamerri Trough (granite). Clay suspensions were diluted in distilled water, disaggregated in an ultrasonic bath, and allowed to dry on carbon-coated copper grids. Further petrographic analyses were carried out XRD on whole-rock and clay separates samples (<2 μm). The XRD analyses were carried out on a Bruker Advance MK III X-Ray diffractometer with Bragg-Brentano geometry and CuKα radiation, operated at 40 kV and 30 mA at a scanning rate of 1min/step and 0.05°/step from 2–32° for oriented clay slides. Polytype analyses were, however, operated at 40 kV and 30 mA at a scanning rate of 30secs/step and 0.05°/step from 16–44° The samples were prepared for separation of the clay fraction by gently crushing the rocks to sand size, followed by disaggregation in distilled water using an ultrasonic bath. Different clay size fractions were obtained by centrifugation, and the decanted suspensions were placed on a glass slide. To ensure no detrital contamination, samples were centrifugally separated and rigorously analysed with XRD. Samples showing contamination with detrital $2M_1$ illite–muscovite were either discarded from analysis or separated to finer micron fractions. Following XRD analysis of air-dried samples, the oriented clay-aggregate mounts were placed in an ethylene–glycol atmosphere at 30–40 °C overnight prior to additional XRD analyses. To determine illite content in illite–smectite mixed-layer clays, the method of differential two-theta (Δ2θ) was used, with an analytical error of about ±5% (Moore and Reynolds, 1997).

3.3. Oxygen and hydrogen stable isotopes

Illitic clay minerals were analysed for their stable isotope ($\delta^{18}O$ and δD) compositions. Oxygen was extracted from illitic clays for isotope analyses using a CO_2-laser and BrF_5 (Sharp, 1990). Oxygen isotope values are reported in per mil relative to V-SMOW and normalised to the international quartz standard (NBS-28) using a value of 9.6‰. Replicate values for NBS-28 quartz (n = 6) analysed with the samples had values that varied by less than 0.2‰. Samples and standards were heated overnight in a muffle furnace to 170 °C prior to loading into the vacuum extraction line to remove any adsorbed water. The samples were then evacuated for approximately 6 hours and left overnight in a vapour of BrF5. Blank BrF_5 was run until the yield was less than 0.1 micro moles oxygen. Oxygen was passed through a fluorine getter (in-line Hg diffusion pump) and converted to CO_2 by a graphite furnace; yields were recorded and CO_2 analysed on a Geo20–20 mass spectrometer at the GNS Laboratory, New Zealand. Hydrogen isotope

analysis of clays was similarly conducted at the GNS Laboratory using a HEKAtech high temperature elemental analyser coupled with a GV Instruments IsoPrime mass spectrometer. All samples were pyrolyzed at 1450°C in silver capsules and analysed in triplicate. All isotope ratios are reported in per mil relative to V–SMOW, with an analytical uncertainty of ±2‰ (1σ). Results are normalised to international standards IAEA–CH–7, NBS30 and NBS22, with reported δD values of –100‰, –66‰ and –118‰, respectively.

3.4. ICP-MS

Clay samples were dissolved with a mixture of HF and nitric acids on a hotplate, then evaporated to dryness, refluxed twice with nitric acid and dissolved in 2 *N* nitric acid. Aliquots of the solutions were spiked with internal standards, diluted and analysed on a Thermo X-series 1 quadrupole inductively coupled plasma mass spectrometer (ICP-MS) in the Radiogenic Isotope Laboratory at the University of Queensland (RIF, UQ). Sample preparation and analytical procedures used were similar to those of Eggins et al. (1997), except that Tm was not used as an internal standard and duplicate low-pressure digestions of W-2, a US Geological Survey diabase standard, were used as the calibration standard. BIR-1, AGV1, AGV2 and G2 were run as unknown. The $^{156}CeO/^{140}Ce$ ratio for the run was 0.016. Long-term precision (RSD) was based on duplicate analyses of the duplicate digestions of AGV1, whilst precision for the run was based on five duplicate analyses of W-2 which were better than 3% for most elements, except for Li, Zn, Mo, Cd, and Cs, which ranged between 5% (Li, Cd and Cs) and 15% (Zn).

3.5. Rb–Sr dating

For the Rb–Sr dating, illitic clay separates were leached for 15 min at room temperature in 1 N distilled HCl (Clauer et al., 1993). Leachate and residue were separated by centrifuging. The residue was rinsed repeatedly with milli-Q water, dried and reweighed. Clay separates were analysed in two separate batches. Leachate, residue, and untreated samples from the first batch were spiked with ^{85}Rb–^{84}Sr mixed tracer and dissolved in a mixture of distilled HF and HNO_3, whilst the second batch were measured directly by Thermo X-series 1 quadrupole ICP–MS with precision better than 0.5% (1σ). The Sr-enriched fraction was separated using cation exchange resins. Sr isotopic ratios were measured on a VG Sector-54 thermal ionisation mass spectrometer (TIMS) in the Radiogenic Isotope Laboratory at University of Queensland. Sr was loaded in TaF_5 and 0.1 *N* H_3PO_4 on a tantalum or tungsten single filament. Sr isotopic ratios were corrected for mass discrimination using $^{86}Sr/^{88}Sr = 0.1194$. Long-term (6 years) reproducibility of statically measured NBS SRM 987 (2σ; *n* = 442) is 0.710249 ± 28. More recent dynamically measured SRM 987 had $^{86}Sr/^{88}Sr$ ratios of 0.710222 ± 20 (2σ; *n* = 140). Rb–Sr isochron ages were calculated using the ISOPLOT program (Ludwig, 2003).

3.6. Sm–Nd dating

Samples chosen for Nd isotope analysis used aforementioned untreated, leachate and acid-leached fractions. These aliquots were separated for Nd following standard cation exchange column chemistry. Neodymium was separated from the REE fraction using Bio Bead® - HDEHP resin and eluting with 0.25 *N* HCl. Nd isotopes were determined using the multi-collector inductively coupled plasma mass spectrometer (MC-ICP-MS) in dynamic mode on a Nu Plasma MC-ICP-MS at RIF, UQ. Nd isotope ratios were corrected for mass fractionation using $^{146}Nd/^{144}Nd = 0.7219$. Repeated measurements of JNdi Nd standard on this mass spectrometer yield an average $^{143}Nd/^{144}Nd = 0.512113 \pm 9$ (2σ; *n* = 11), which is consistent with a consensus value of 0.512115 ± 7 (Tanaka et al., 2000). An in-house lab standard, Ames Nd Metal was used as a routine instrument drift monitor, correspondent with JNDi-1, 17 analyses yield an average of $^{143}Nd/^{144}Nd = 0.511966 \pm 16$. This value was used as calibration reference for instrument drift, which is usually less than 15ppm. The Nd procedural blank is ~50 pg.

3.7. Ar–Ar dating

A total of 5 samples from the Nappamerri Trough were dated by the Ar–Ar method at the University of Michigan. Illitic clay samples were resuspended in 1 mL of deionized water, spun-down at 10,000 rpm in a microcentrifuge and carved into a ~1mm pellet following decanting. To avoid loss of ^{39}Ar due to recoil, clay pellets were placed in 1mm ID fused silica vials prior to being sent for neutron irradiation for 90MWh in medium flux locations of the McMaster Nuclear Reactor (hole 8C for irradiation 1, 8A for irradiation 2). Following irradiation, samples were attached to a laser fusion system, broken under a 1×10^{-8} Torr vacuum and step-heated *in situ* using a defocused beam from a 5 W Coherent Innova continuous Ar-ion laser operated in multi-line mode. Argon isotopes were then analysed using a VG1200S mass spectrometer equipped with a Daly detector operated in analogue mode using methods by Hall (2013). Ages in this study are calculated relative to an age of 520.4 Ma for standard hornblende MMhb-1(Samson and Alexander, 1987).

4. RESULTS

4.1. Petrography

In thin section, the majority of granite samples examined show intense illitic alteration resulting in almost complete destruction and replacement of feldspars and primary mica, representing ≥ 50% of the whole-rock (Fig. 1a). Accessory phases (identified with SEM–EDS) similarly show intense alteration, as seen from varying destruction of primary zircon [$ZrSiO_4$]. Zircon appears with xenotime [$HREEPO_4$], + thorite [$ThSiO_4$] overgrowths along partially metasomatised rims or as almost completely altered subhedral remnants intergrown with xenotime, thorite, and/or bastnaesite (Fig. 1b; [$LREE(CO_3)F$]). Examples of monazite [$LREEPO_4$] and coffinite [$U(SiO_4)_x(OH)_{4x}$] are found sporadically in altered samples. Illite also occurs as pervasive veinlet networks commonly associated with Th-rich colloform bastnaesite, as identified with energy dispersive X-ray spectroscopy. The deepest sample (McL1_3749.1), however, shows less intense alteration of primary feldspars and mica, with no evidence of illite veining. Analysis of highly altered samples with field emission gun–SEM reveals two generations of illite recognisable by grain size and morphology. One generation is distinguished by large (up to 100 μm), lath-shaped crystals with convoluted compositional zonation, identified with EDS. A cross-cutting generation, however, shows no identifiable chemical zonation and forms fine needle-like grains (1–2 μm). Other alteration products include ankerite–siderite (confirmed by XRD) rimmed by akaganeite [Fe(OH,Cl)] intergrown with tabular bastnaesite and fluorite. Quartz is found as primary subhedral and microcrystalline grains.

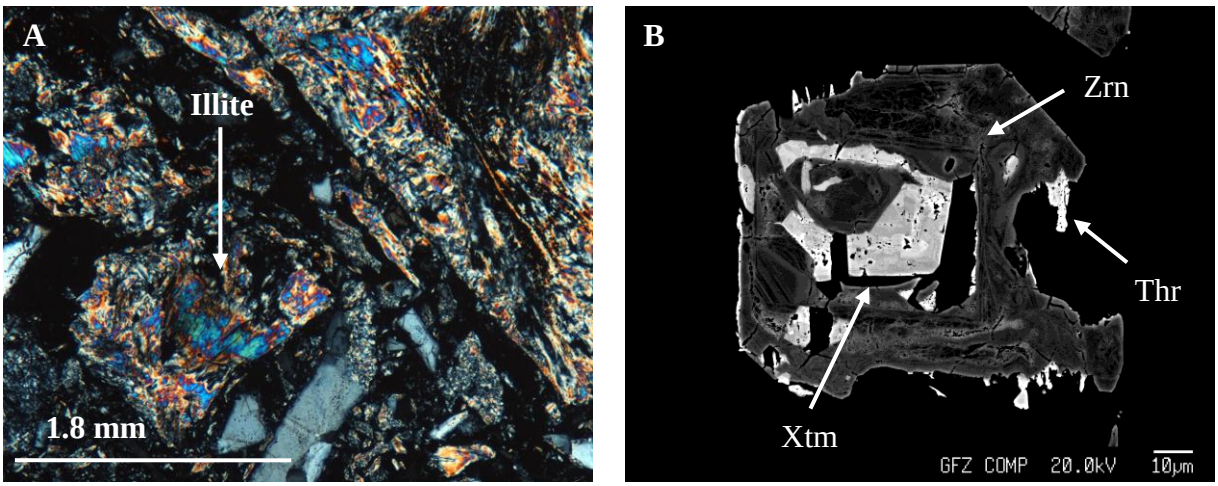

Figure 1. Cross-polarised light photomicrograph of illite-rich alteration of Big Lake Suite granite replacing primary feldspars and micas (A), and back-scatter electron (BSE) image of altered zircon (Zrn) intergrown with xenotime (Xtm) and thorite (Thr).

4.2. Geochronology of illitic clays from the Nappamerri Trough

4.2.1. Sm–Nd dating

A summary of all age data can be found in Figure 2. Samarium and neodymium isotopic analyses were carried out on selected untreated and acid-leached aliquots from MB_72 granite-hosted illite samples. Samples were chosen on the basis of highly variable rare earth element compositions to give a wide enough range of Sm/Nd ratios appropriate for this dating method (Peng et al., 2003). When plotted together, samples produce a meaningful $^{147}Sm/^{144}Nd$–$^{143}Nd/^{144}Nd$ isochron. Samples show a non-linear relationship on a 1/Nd vs. $^{143}Nd/^{144}Nd$ diagram, therefore eliminating the possibility the age data represent a two-fluid mixing-line. The isochron age is 128 ± 16 Ma (2σ) with an intercept of 0.512212 ± 17 (initial εNd = –8.3). Using measured $^{143}Nd/^{144}Nd$ values and the acquired Cretaceous age, Nd isotopic compositions were calculated for the time of formation. The initial isotopic values in the epsilon (ε) notation use calculations after McCulloch and Wasserburg (1978) with $^{147}Sm/^{143}Nd$ CHUR (Chondritic Uniform Reservoir), present = 0.1967 (Jacobson and Wasserburg, 1980) and $^{143}Nd/^{144}Nd$ CHUR = 0.512638 (Goldstein et al., 1984). $\varepsilon Nd_{(128)}$ values vary minimally and range from –5.6 to –4.9.

4.2.2. Rb–Sr dating

Data from granite and sediment-hosted acid-leached residue clay fractions produced two linear relationships corresponding to of 86.6 ± 2.3 Ma (initial 0.7678 ± 0.0095; MSWD = 2.0) and 94.7 ± 4.2 Ma (initial $^{87}Sr/^{86}Sr$ = 0.824 ± 0.022; MSWD = 0.40) with the latter made of samples wholly from MB72. Selected leachate and untreated aliquots from MB_72 and BL_1 with anomalously high Sr^{87}/Sr^{86} values (0.9161 – 1.0357) produce a well-defined linear relationship with a mid Cretaceous age of 94.2 ± 1.8 Ma (initial Sr^{87}/Sr^{86} = 0.91357 ± 0.00091; MSWD = 1.9) and are parallel to the MB72 isochron.

4.2.3. Ar–Ar dating

Five granite-hosted illite samples of similar illite crystallinities were analysed for $^{40}Ar/^{39}Ar$ geochronology. Samples show small degrees of low temperature ^{39}Ar "recoil loss", 9.5–10.8%, typical for well crystalline illite grains (Hall et al., 1997). Age data (1σ) is provided as total-gas or retention ages (Dong et al., 1995).The total-gas age refers to that produced from all the gas release from encapsulated samples, whilst the "retention age" is the apparent $^{40}Ar/^{39}Ar$ age derived from all gases, excluding the first room-temperature gas fraction (recoil) in a vacuum-encapsulation experiment (Dong et al., 1995; Hall, 2013). Separates of 2–0.5µm fraction from MB1_2847.75 and MB1_2857.4 provide the youngest total-gas and retention ages of 93.3 ± 0.4 Ma and 102.8 ± 0.4 Ma, and 82.9 ± 0.6 Ma and 96.4 ± 0.7 Ma, respectively. Total degassing ages of MB_72 clays range from 96.6 ± 0.5 Ma to 102.3 ± 1.1 Ma with the oldest age belonging to the coarsest clay fraction of 1–2µm. All samples have well developed plateaus attributed to discrete thermal episodes (Haines and Van de Pluijm, 2010). However, such plateaus do not necessarily represent geologically significant ages as heat-spectra can be adversely affected by recoil and the presence of point defects (Hall et al., 2000).

4.3. Stable isotope chemistry

Most granite-hosted illites have $\delta^{18}O$ values from 1.2‰ to 2.7‰, while $\delta^{18}O$ values of almost all sediment-hosted clay minerals range from 4.9‰ to 9.7‰. One granite-hosted sample from the Big Lake 1 drill hole does, however, have an anomalously depleted $\delta^{18}O$ value of –1.8‰. Most granite- and sediment-hosted samples exhibit δD values ranging from –110‰ to –83‰ and –116‰ to –86‰, respectively. Four clay samples from the McLeod and Big Lake drill holes, although exhibiting typical oxygen values (1.7‰ to 8.5‰), show unusually depleted δD values of –121‰ to –116‰. Calculated fluid isotopic values for granite-hosted samples vary from –5.6‰–0.2‰ for $\delta^{18}O$ and –115‰ to –73.8‰ for δD, whereas sediments-hosted samples give values of –5.3‰ to 4.2‰ and –105‰ to –74.6‰, respectively. Two main populations (A and B) exist when all calculated δD and $\delta^{18}O$ fluid isotopic values are plotted in a δD–$\delta^{18}O$ diagram (Figure 3**)**.These populations comprise stratigraphically shallower samples with average δD values of –86‰ (Pop. A) and deeper samples with more negative δD values (average = –112‰; Pop. B).

4.4. Trace element data

UCC-normalised diagrams of granite-hosted, acid-leached residue mimic that of the whole-rock pattern presenting marginally LREE-rich to flat patterns with pronounced negative Eu-anomalies. Larger grain size fractions (< 2 and 2–1 μm) show minor enrichment in LREE to flat normalised patterns, whereas finer size fractions (< 1 and < 0.5 μm) are relatively LREE depleted. Rare earth element patterns for residue separates that produced a ~86 Ma isochron are consistently marked by a prominent negative Ce-anomaly**.** Comparatively LREE-depleted patterns are produced for older untreated and leachate separates from the Moomba 72 and Big Lake 1 drillholes, which define a ~94 Ma isochron. It should also be noted that Th concentrations of residue separates are substantially higher than typical basinal illite (Rousset and Clauer, 2003) and account for ~50% of whole-rock Th. An estimation of 50% is based on the observation that ≥ 50% of the granitic samples are altered to illite. UCC-normalised trace element diagrams similarly show acid-leached residue with comparable to elevated Th concentrations relative to unaltered granite.

5. DISCUSSION

5.1. Geological implications of illite ages

Integrated geochronology indicates that only the Nappamerri Trough underwent episodic fluid flow for ~35 Myr (~128–86 Ma) during the Cretaceous, which was most likely localised along reactivated fault systems (Mavromatidis, 2008). This period is coincident with previous thermochronological studies that record a substantial thermal "recrystallisation event" of K-feldspar from the BLS, at ≤260°C from 120–80 Ma, which is attributed to "rapid sediment accumulation and probably structural modification" (McLaren and Dunlap, 2006). Such thermal perturbations (≤ 350 °C) were also recognised from ~100–85 Ma and resulted in the maturation–expulsion of substantial quantities of hydrocarbons into the dry-gas zone (Kantsler et al., 1978; Deighton and Hill, 1998). Maturation of kerogen to this extent is can be produced from either a long-lasting diagenetic event of a high-temperature short-term thermal episode consistent multiple stages of Cretaceous tectonism (Derkowski et al., 2013). An elevated thermal regime associated with extension and an influx of hydrothermal evolved meteoric fluids may, therefore, have provided sufficient heat to stimulate both hydrocarbon expulsion and K-feldspar recrystallisation (Allen and Allen, 2005). Further evidence of extensional tectonism is seen from widespread normal faults throughout mid-Cretaceous Winton and Mackunda fomartions of the Eromanga Basins (Mavromatidis, 2008) as well as thickening of the volcanogenic, Winton Fm(Cook et al., 2013), which was dated at ~105–95 Ma from detrital zircon studies (Bryan et al., 2012). The Cretaceous illites ages are consistent with extensive rifting of the southern and eastern margins of Australia, concomitant with emplacement of the Whitsunday silicic large igneous province (130–95 Ma; Bryan et al., 2012) (Fig. 2). Rifting along the eastern Australian margin (>2500 km) east of the study area was initiated suddenly at ~125–120 Ma along a N–S orientated volcanic rift system (Bryan et al., 1997), coincident with our Sm–Nd age of 128 ± 16 Ma.

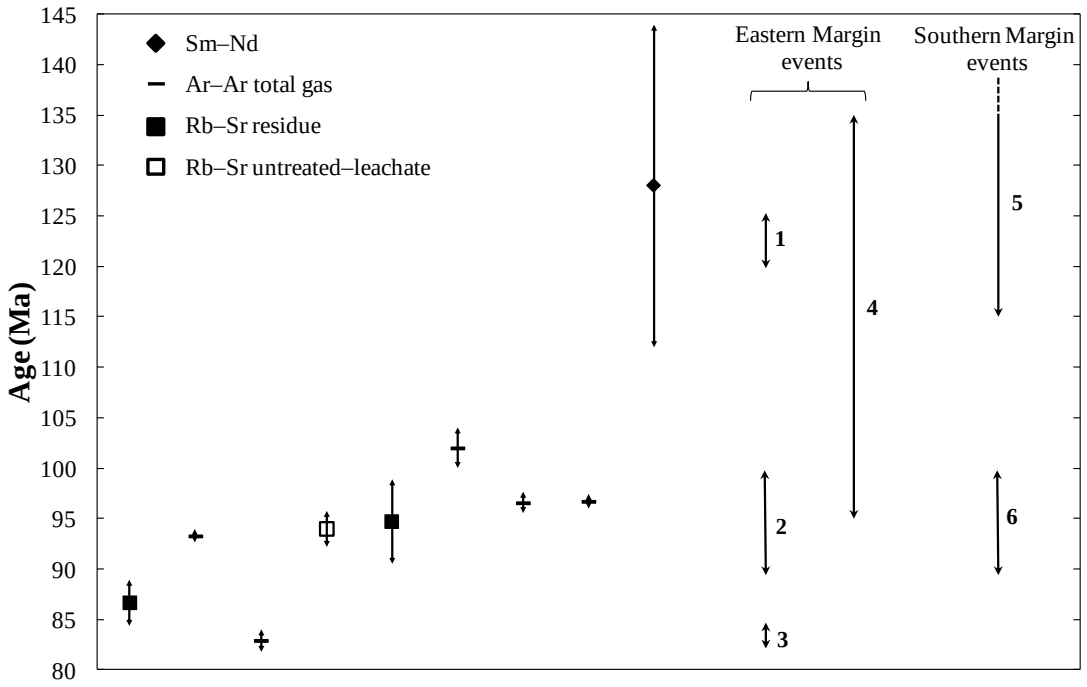

Figure 2. Chronological chart showing consistency of Sm–Nd, Rb–Sr and Ar–Ar dating with rifting of the southern and eastern margins of Australia and opening of the Tasman Sea. The numbers refer to previously reported events as follows: (1) initiation of rifting along the southern margin (Bryan et al., 2012), (2) accelerated rifting and exhumation of the eastern margin (O'Sullivan et al., 1995), (3) opening of the Tasman Sea (Veevers et al., 1991), (4) emplacement of the Whitsunday silicic large igneous province (Bryan et al., 2012), (5) rifting of the southern margin of Australia (Williamson et al., 1990) and (6) break-up of the southern continental margin (Veevers, 1986).

~94 Ma ages provided by 1–2 µm Ar–Ar and Rb–Sr data are also in agreement with accelerated rifting and exhumation beginning at ~100 Ma along the eastern margin (O'Sullivan et al., 1995). The youngest generation of illite, dated between ~82 and ~86 Ma similarly coincides with rupture of the continental crust and onset of Tasman sea-floor spreading (~84 Ma; Veevers et al., 1991; Bryan et al., 2012) that was similarly recorded by Rb–Sr dating in the Gunnedah basin system of eastern Australia (~86 and 94 Ma; Uysal et al., 2011b). Episodic fluid flow is also suggested by the depth-related distribution of radiometric ages in the BLS granite. As ~86 Ma illites are predominantly isolated to depths of ~2850 m, the 94 Ma fluid flow event may have sufficiently reduced permeability restricting subsequent circulation of fluids to shallower more permeable areas of the granite.

Chronological consistency with Gondwana rifting may suggest plate-wide transmission of tensional stress, commonly associated with break-up and dispersal, to previous thermally and mechanically weakened lithosphere (Coblentz and Sandiford, 1994; Friedmann and Burbank, 1995; Armitage and Allen, 2010). Thermal weakening of the Warburton–Cooper basins likely derives from high geothermal gradients associated with emplacement and high radiogenic heat flow of the Big Lake Suite. On the other hand, mechanical weakening may stem from episodic compression–extension that lead to the formation of the GMI Ridge and accommodated emplacement of the Big Lake Suite granite (Sonder et al., 1987; Braun and Beaumont, 1989). This hypothesis is also consistent with quantitative modelling of Müller et al. (2012) who showed that localised intraplate structural events of the Cretaceous derive from interaction of far field stresses with particularly weak zones of the Australian continent.

5.2. Stable isotopes

Calculated $\delta^{18}O$ fluid values are consistent with illite precipitation from evolved mid- to high-latitudinal Cretaceous meteoric waters (Veevers, 1984). The population with more negative δD values, however, is unlikely to have resulted from typical evolution of waters away from the meteoric water line, as calculated isotopic compositions are below that expected for Cretaceous meteoric water (cf., Uysal et al., 2011). The presence of two populations in the Nappamerri fluid values (Fig. 3) may result from an evolving meteoric fluid with a divergent isotopic trajectory. Less negative fluid δD values shown by samples along the upturned trend (Pop. A) are compatible with isotopic exchange with hydrogen-rich minerals under low fluid/rock ratios (Fig. 6; Yardley et al., 1991; Uysal et al., 2000). In contrast, a downturned isotopic trend to more negative fluid δD and somewhat more positive fluid $\delta^{18}O$ values for population B may indicate a decoupling of the hydrogen and oxygen isotopic systems at depth. The expulsion of hydrocarbons during the lower Cretaceous may offer an explanation, as organic material acts as a substantial source of isotopically light hydrogen (Ziegler et al., 1994; Polya et al., 2000). Previous studies have shown that hydrothermal interaction processes are efficient at organic maturation of hydrocarbons during which substantial volatiles and soluble compounds are lost (Didyk and Simoneit, 1989; Simoneit, 1992). More negative mineral and fluid δD values with depth may suggest that increasing fluid temperatures resulted in more intense alteration–maturation of organic matter.

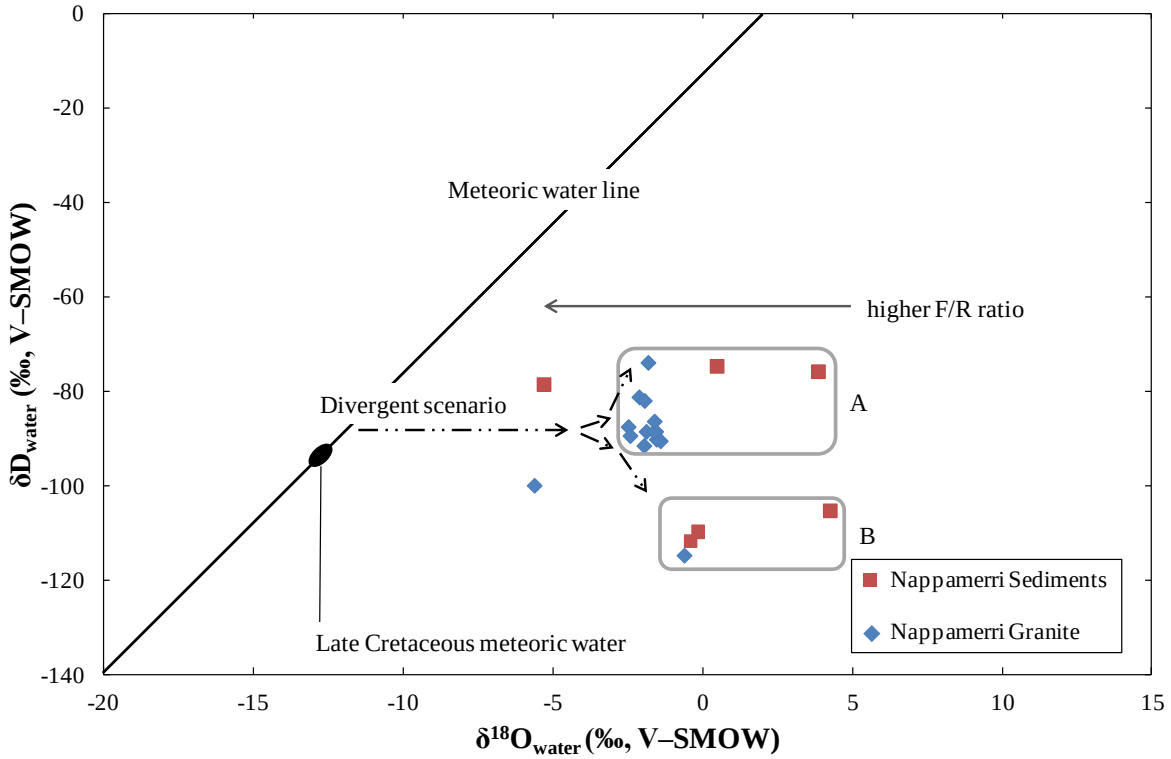

Figure 3. Calculated $\delta^{18}O$ and δD fluid values in equilibrium with illite-rich clays from the Nappamerri Trough relative to Late Cretaceous meteoric water (c.f. Uysal et al., 2011). Two distinct populations, labelled as A and B, comprise stratigraphically shallower samples with average δD values of –86‰ (Pop. A) and deeper samples with more negative δD values (average = –112‰; Pop. B).

This would have contributed a larger proportion of D-depleted hydrogen to the fluid phase prior to the alteration of granite and precipitation of illite (Fig. 7; Ziegler et al., 1994; Girard et al., 2002). This suggestion is also compatible with widespread hydrocarbon maturation within the Cooper Basin, correlated with an anomalous thermal event in the Late Cretaceous (Deighton and Hill, 1998). The slightly more positive fluid $\delta^{18}O$ values of population B with depth cannot realistically result from decreasing temperature, as indicated by estimated palaeotemperatures calculated from previous vitrinite reflectance data (Fig. 5; Kantsler et al., 1978). Assuming negligible detrital phase contamination, a more plausible explanation is that elevated fluid $\delta^{18}O$ values result from fluid-rock interaction with ^{18}O-rich phases under low fluid/rock ratios at depth. A pattern of more negative δD and more positive $\delta^{18}O$ values with indicates decoupling of the isotopic systems. Variations in hydrogen appear to reflect temperature-dependent fluid–rock interaction with organics, while variations in $\delta^{18}O$ values are independent of temperature and are affected by varying fluid/rock ratios. Anomalously negative $\delta^{18}O$ values in the Big Lake drill holes are likely due to fluid–rock interactions under considerably higher fluid/rock ratios (cf. Uysal et al., 2000). Isotopically heavier $\delta^{18}O$ values of some sediment-hosted clays are consistent with extensive oxygen isotopic exchange, under lower fluid/rock ratios, between higher temperature hydrothermal fluids and sedimentary assemblages, as seen in geothermal systems of extensional environments (Truesdell and Hulston, 1980).

5.3. Trace element data

Differential mobility of trace elements, such as REE, in hydrothermal solution depends on parameters such as fluid composition and redox state (Wood, 1990; Bau, 1991). The presence of negative Ce-anomalies throughout UCC-normalised patterns from ~86 Ma residues of illites from the Nappamerri Trough is testament to this, and allows distinction from ~94 Ma residues. Such anomalies can develop from a change in valency of Ce (Ce^{3+} to Ce^{4+}) in oxidising conditions to form insoluble cerianite (CeO_2) that will fractionate from the remaining, more mobile REE^{3+} (Bau, 1991; Bau and Möller, 1992; Uysal et al., 2011a). Leachates and untreated separates from Moomba 72 can similarly be differentiated by their anomalous UCC-normalised REE and trace element patterns. As Moomba 72 residue samples are not anomalous, trace element composition for untreated separates must relate to the contribution from the leachable phases.

It should be noted that the most altered granite samples contain the highest concentrations of Th, with illite accounting for ~40–50% of the total budget, while the remaining Th likely resides predominantly in accessory phases, such as bastnaesite, monazite or coffinite. Uranium concentrations are, however, maintained in altered and unaltered samples, which may infer reducing conditions incapable of mobilising U^{4+}. Thorium-enriched illite suggests that illitising hydrothermal fluids were able to leach and/or mobilise substantial concentrations of Th from elsewhere within the granitic body. Alternatively, as unaltered BLS granite hosts lower Th content than its altered counterpart, Th may have been mobilised from the surrounding country-rock. This seems likely as preceding uplift and glacial erosion of the granite lead to shedding of HPE-enriched detritus into surrounding lithologies, such as the "Tirrawarra Conglomerate" (Meixner et al., 1999). As such, episodic influxes of Cretaceous hydrothermal fluids carrying high concentrations of Th, could actively affect the budget of heat-producing elements in the Big Lake Suite granite. This phenomenon is compatible with the work of Martin (2006), who suggested that unusually high concentrations of HFSE, REE and HPE in anorogenic granites relate to protracted interaction of fenitising hydrothermal fluids with the crust during magma emplacement.

5.4. Implications for the formation of highly radiogenic granites and its influence on enhanced geothermal system exploration

A-type or anorogenic granites can have especially high concentrations of heat-producing elements if their parent melt derives from a metasomatised and previously enriched crustal source (Martin, 2006; Bea, 2012). Crustal enrichment results from multiple influxes of mantle-sourced, volatile-rich fluids. Such fluids can escape from a rising asthenospheric plume in an anorogenic setting, leach high field-strength and rare earth elements from the surrounding rock and enrich areas of the lower crust (Woolley, 1987; Martin, 2006).

Vein and authigenic mineral phases sampled from the Warburton–Cooper–Eromanga basins record multiple tectonic events that allowed an influx of hydrothermal fluids (Middleton et al., 2013). Illite specifically records five events in the Carboniferous, Jurassic and Cretaceous. The Big Lake Suite granite is pervasively altered, with illite comprising ~50% of the rock mass. Trace element analyses of illite samples show that residue fractions have Th and U concentrations up to 93 ppm and 25 ppm, respectively. In some samples, illite contributes to ~50% of the heat-producing nature of the granite. This implies that fluids capable of altering the granite were laden with radiogenic elements potentially leached from the surrounding country-rock and granite. The implications of this observation are two-fold. The first is that under certain hydrothermal conditions, Th is substantially more mobile than previously thought. The second is that episodic hydrothermal mobilisation of heat-producing elements may offer an alternative, metasomatic origin to the unusual enrichment of the BLS in radiogenic elements. Similar observations were noted by in the Galiñeiro orthogneissic complex of north-western Spain (Montero et al., 1998). Montero et al. (1998) recorded extremely high concentration of elements, such as Th (up to 7223 ppm), localised in areas displaying evidence of metasomatic processes. Extreme incompatible element enrichment was attributed to "episodic metasomatic mobilisation" by volatile-rich (F, CO_2, S_2) fluids driven by multiple phases of orogenic metamorphism.

Analysis of secondary mineral phases clearly offers a potential tool during exploration for enhanced geothermal systems. Conducting geochemical and geochronological analysis on authigenic illite can determine the presence of episodic fluid flow and whether fluids were capable of mobilising radiogenic elements. Therefore, if an anorogenic granite is highly altered and has experienced multiple periods of hydrothermal interaction with radiogenic element-rich fluids, it may represent a high-priority target for geothermal energy utilisation.

6. CONCLUSIONS

This study utilised geochronological, trace element and stable isotopic analyses of authigenic illite to constrain successive hydrothermal events in the Warburton–Cooper basins. Samples from the Nappamerri Trough indicate episodic circulation of evolved meteoric waters under variable fluid/rock ratios and high geothermal gradients in the Cretaceous (~100 $°Ckm^{-1}$). As the

Warburton–Cooper basins lie considerable distances from active plate margins, recorded tectonism likely derives from localisation of far-field stresses to thermally and mechanically weakened regions of the Australian continent. Such weaknesses may stem from continual reactivation of fault networks as well as considerable heat-flow from the highly radiogenic Big Lake suite granite.

The influx of moderate-temperature hydrothermal fluids had a significant effect on the surrounding geology leading to the maturation–expulsion of hydrocarbons and substantial enrichment of the BLS granite in Th. This work provides temporal and chemical constraints on the formation of two of Australia's more prolific energy resources Furthermore, by combining mineralogical, chemical and previous chronological analyses this study provides the most comprehensive and holistic record of the thermal, tectonic and fluid flow evolution of one of the world's more enigmatic basin systems.

REFERENCES

Allen, P. A. and Allen, J. R., 2005. *Basin analysis: principles and applications*. Blackwell Science Ltd., Oxford.

Apak, S. N., Stuart, F., Lemon, N. M., and Wood, G., 1997. Structural evolution of the Permian–Triassic Cooper Basin, Australia: Relation to hydrocarbon trap styles. *AAPG Bulletin* **81**, 533–555.

Apak, S. N., Stuart, W. J., and Lemon, N. M., 1995. Compressional control on sedimentation and facies distribution SW Nappamerri Syncline and adjacent Murteree High, Cooper Basin. *The APEA Journal* **35**, 190-202.

Armitage, J. J. and Allen, P. A., 2010. Cratonic basins and the long-term sibsidence history of continental interiors. *Journal of the Geological Society* **167**, 61–70.

Bau, M., 1991. Rare-earth element mobility during hydrothermal and metamorphic fluid-rock interaction and the significance of the oxidation state of europium. *Chem. Geol.* **93**, 219–230.

Bau, M. and Dulski, P., 1995. Comparative study of yttrium and rare-earth element behaviours in fluorine-rich hydrothermal fluids. *Contrib. Mineral. Petr.* **119**, 213–223.

Bau, M. and Möller, P., 1992. Rare Earth Element Fractionation in Metamorphogenic Hydrothermal Calcite, Magnesite and Siderite. *Mineral. Petrol.* **45**, 231–246.

Bau, M., Romer, R. L., Lüders, V., and Dulski, P., 2003. Tracing element sources of hydrothermal mineral deposits: REE and Y distribution and Sr-Nd-Pb isotopes in fluorite from MVT deposits in the Pennine Orefield, England. *Miner. Deposita* **38**, 992–1008.

Bea, F., 2012. The sources of energy for crustal melting and the geochemistry of heat-producing elements. *Lithos* **153**, 278–291.

Braun, J. and Beaumont, C., 1989. Contrasting styles of lithospheric extension: Implications for differences between the Basin and Range province and rifted continental margins. In: Tankard, A. J. and Balkwill, H. R. Eds.), *Extensional Tectonics and Stratigraphy of the North Atlantic Margin*. AAPG.

Bryan, S. E., Constantine, A. E., Stephens, C. J., Ewart, A., Schön, R. W., and Parianos, J., 1997. Early Cretaceous volcano-sedimentary successions along the eastern Australian continental margin: Implications for the break-up of eastern Gondwana. *Earth Planet. Sci. Lett.* **153**, 85–102.

Bryan, S. E., Cook, A. C., Allen, C. M., Siegel, C., Purdy, D., Greentree, J. S., and Uysal, I. T., 2012. Early–mid Cretaceous tectonic evolution of eastern Gondwana: From silicic LIP magmatism to continental rupture. *Episodes* **35**, 142–152.

Chopra, P. and Wyborn, D., 2003. Australia's first hot dry rock geothermal energy extraction project is up and running in granite beneath the Cooper Basin, NE South Australia*The Ishihara Symposium: Granites and Associated Metallogenesis*, Macquarie, Australia.

Clauer, N., Chaudhuri, S., Kralik, M., and Bonnotcourtois, C., 1993. Effects of experimental leaching on Rb–Sr and K–Ar isotopic systems and REE contents of diagenetic illite. *Chem. Geol.* **103**.

Coblentz, D. D. and Sandiford, M., 1994. Tectonic stresses in the African plate: Constraints on the ambient lithospheric stress state. *Geology* **22**, 831–834.

Cook, A. G., Bryan, S. E., and Draper, J. J., 2013. Post-orogenic Meoszoic basins and magmatism. In: Jell, P. A. (Ed.), *Geology of Queensland*. Geological society of Queensland, Brisbane.

Deighton, I. and Hill, A. J., 1998. Thermal and burial history. In: Gravestock, D. I., Hibburt, J., and Drexel, J. F. Eds.), *Petroleum Geology of South Australia*. South Australia. Department of Primary Industries and Resources.

Derkowski, A., Bristow, T. F., Wampler, J. M., Środoń, J., Marynowski, L., Elliot, W. C., and Chamberlain, C. P., 2013. Hydrothermal alteration of the Ediacaran Doushantuo Formation in the Yangtze Gorges area (south China). *Geochim. Cosmochim. Acta* **107**, 279–298.

Didyk, B. M. and Simoneit, B. R. T., 1989. Hydrothermal oil of Guaymas Basin and implications for petroleum formation mechanisms. *Nature* **65–69**.

Dong, H., Hall, C. M., Peacor, D., and Halliday, A. N., 1995. Mechanisms of argon retention in clats revealed by laser ^{40}Ar–^{39}Ar dating. *Science* **267**, 355–359.

Eggins, S. M. W., J. D., Kinsley, L. P. J. M., G. E., Sylvester, P., McCulloch, M. T., Hergt, J. M., and Handler, M. R., 1997. A simple method for the precise determination of ≥ 40 trace elements in geological samples by ICPMS using enriched isotope internal standardisation. *Chem. Geol.* **134**, 311–326.

Friedmann, S. J. and Burbank, D. W., 1995. Rift basins and supradetachment basins: intracontinental extensional end-members. *Basin Res.* **7**, 109–127.

Gatehouse, C. G., 1986. The geology of the Waburton Basin in South Australia. *Aust. J. Earth Sci.* **33**, 161–180.

Gatehouse, C. G., Fanning, C. M., and Flint, R. B., 1995. Geochronology of the Big Lake Suite, Warburton Basin, northeastern South Australia*Quarterly Geological Notes*. Geological Survey of South Australia.

Girard, J.-P., Munz, I. A., Johansen, H., Lacharpagne, J.-C., and Sommer, F., 2002. Diagenesis of the Hild Brent Sandstones, Northern North Sea: Isotopic Evidence for the Prevailing Influence of Deep Basinal Water. *Journal of Sedimentary Research* **72**, 746-759.

Haines, S. H. and Van de Pluijm, B. A., 2010. Dating the detachment fault system of the Ruby Mountains, Nevada: Singinficance for the kinematics of low-angle normal faults. *Tectonics* **29**, TC4028.

Hall, C. M., 2013. Direct measurement of recoil effects on $^{40}Ar/^{39}Ar$ standards. In: Jourdan, F., Mark, D. F., and Verati, C. Eds.), *Advances in $^{40}Ar/^{39}Ar$ dating: from Archaeology to Planetary Sciences*. Geological Society, London.

Hall, C. M., Higueras, P. L., Kesler, S. E., Lunar, R., Dong, H., and Halliday, A. N., 1997. Dating of alteration episodes related to mercury mineralisation in the Almadén district, Spain. *Earth Planet. Sci. Lett.* **148**, 287–298.

Hall, C. M., Kesler, S. E., Simon, G., and Fortuna, J., 2000. Overlapping Cretaceous and Eocene alteration, Twin Creeks Carlin-type deposit, Nevada. *Econ. Geol.* **95**, 1739–1752.

Hillis, R. R., Hand, M., Mildren, S., Morton, J., Reid, P., and Reynolds, S., 2004. Hot dry rock geothermal exploration in Australia*PESA Eastern Australian Basins Symposium II*, Adelaide.

Kantsler, A. J., Cook, A. C., and Smith, G. C., 1978. Rank variation, calculated palaeotemps understanding oil, gas occurrence. *Oil and Gas Journal* **Nov. 20**, 196–205.

Kuang, K. S., 1985. History and style of Cooper–Eromanga Basin structures. *Exploration Geophysics* **16**, 245–248.

Kyser, T. K., 2007. Fluids, basin analysis, and mineral deposits. *Geofluids* **4**, 238-257.

Longstaffe, F. J., 2000. An introduction to stable oxygen and hydrogen isotopes and their use as fluid tracers in sedimentary systems. In: Kyser, K. (Ed.), *Fluids and Basin Evolution*. Mineralogical Association of Canada, Ottawa.

Ludwig, K. R., 2003. *Users manual for ISOPLOT/EX, version 3. A geochronological toolkit for Microsoft Excel.* Berkeley Geochronological Centre Special Publication.

Marshall, V. J., 2013. Petrological, geochemical and geochronological characterisation of heat-producing granites. MPhil, University of Queensland.

Martin, R. F., 2006. A-type granites of crustal origin ultimately result from open-system fenitization-type reactions in an extensional environment. *Lithos* **91**, 125–136.

Mavromatidis, A., 2006. Burial/exhumation histories for the Cooper-Eromanga Basins and implications for hydrocarbon exploration, Eastern Australia. *Basin Res.* **18**, 351–373.

Mavromatidis, A., 2008. Two layer model of lithospheric compression and uplift / exhumation in an intracratonic setting: an example from the Cooper–Eromanga Basins, Australia. *International Journal of Earth Science* **97**, 623–634.

McLaren, S. and Dunlap, W. J., 2006. Use of $^{40}Ar/^{39}Ar$ K-feldspar thermochronology in basin thermal history reconstruction: an example from the Big Lake Suite granites, Warbruton Basin, South Australia. *Basin Res.* **18**, 189–203.

Meixner, A. J., Boucher, R. K., Yeates, A. N., Gunn, P. J., Richardson, L. M., and Frears, R. A., 1999. Interpretation of geophysical and geological data sets, Cooper Basin region, South Australia. Australian Geological Survey Organisation.

Middleton, A. W., Uysal, I. T., Bryan, S. E., Hall, C. M., and Golding, S. D., 2013. Crustal evolution of the intracontinental Warburton–Cooper–Eromanga Basin system, central Australia. *Mineralogical Magasine* **77**, 1754.

Middleton, A. W., Uysal, I. T., Golding, S. D., Förster, H.-J., and Rhede, D., under review. Integrated geochronology and geochemistry from the Waburton Basin, Australia: Deciphering a thermal history. *Chem. Geol.*

Montero, P., Floor, P., and Corretgé, G., 1998. The accumulation of rare-earth and high field-strength elements in peralkaline granitic rocks: The Galiñeiro orthogneissic complex, north-western Spain. *Can. Mineral.* **36**, 683–700.

Moore, D. M. and Reynolds, R. C. J., 1997. *X-ray Diffraction and the Identification and Analysis of Clay Minerals*. Oxford University Press, Oxford.

Müller, R. D., Dyksterhuis, S., and Rey, P., 2012. Australian paleo-stress fields and tectonic reactivation over the past 100 Ma. *Aust. J. Earth Sci.* **59**, 13–28.

O'Sullivan, P. B., Kohn, B. P., Foster, D. A., and Gleadow, A. J. W., 1995. Fission track data from the Bathurst Batholith: evidence for rapid mid-Cretaceous uplift and erosion within the eastern highlands of Australia. *Aust. J. Earth Sci.* **42**, 597–607.

Peng, J.-T., Hu, R.-Z., and Burnard, P. G., 2003. Samarium–neodymium isotope systematics of hydrothermal calcites from the Xikuangshan antimony deposit (Hunan, China): the potential of calcite as geochronometer. *Chem. Geol.* **200**, 129–136.

Polya, D. A., Foxford, K. A., Stuart, F., Boyce, A. J., and Fallick, A. E., 2000. Evolution and paragenetic context of low δD hydrothermal fluids from the Panasqueira W–Sn deposit, Portugal: New evidence from microthermometric, stable isotope, noble gas and halogen analyses of primary fluid inclusions. *Geochim. Cosmochim. Acta* **64**, 3357–3371.

Reuter, A. and Dallmeyer, R., 1987. Significance of Ar40/Ar39 age spectra of whole-rock and constituent grain-size fractions from anchizonal slates. *Chem. Geol.* **66**, 73–88.

Roberts, D. C., Carroll, P. G., and Sayers, J., 1990. The Kalladeina Formation - A Warburton Basin Cambrian carbonate play. *The APEA Journal* **30**, 166–184.

Rousset, D. and Clauer, N., 2003. Discrete clay diagenesis in a very low-permeable sequence constrained by an isotopic (K–Ar and Rb–Sr) study. *Contrib. Mineral. Petr.* **145**, 182–198.

Samson, S. D. and Alexander, E. C. J., 1987. Calibration of the interlaboratory 40Ar/39Ar dating standard, MMhb-1. *Chemical Geology Isotope Geoscience* **66**.

Sharp, Z. D., 1990. Laser-based microanalytical method for the in situ determination of oxygen isotope ratios of silicates and oxides. *Geochim. Cosmochim. Acta* **54**.

Simoneit, B. R. T., 1992. Organic matter alteration and fluid migration in hydrothermal systems. In: Parnell, J. (Ed.), *Geofluids: Origin, Migration and Evolution of Fluids in Sedimentary Basins*. Geological Society Special Publication, London.

Sonder, L. J., England, P. C., Wernicke, B. R., and Christiansen, R. L., 1987. A physical model for Cenozoic extension of western North America. In: Coward, M. P., Dewey, J. F., and Hancock, P. L. Eds.), *Continental Extensional Tectonics*. Special Publication fo the Geological Society.

Sun, X., 1997. Structural style of the Warburton Basin and control in the Cooper and Eromanga Basins, South Australia. *Exploration Geophysics* **28**, 333–339.

Sun, X., 1999. Fracture analysis of the Eastern Warburton Basin (Early Proterozoic), South Australia. Primary Industries and Resources, South Australia.

Tanaka, T., Togashi, S., Kamioka, H., Amakawa, H., Kagami, H., Hamamoto, T., Yuhara, M., Orihashi, Y., Yoneda, S., Shimizu, H., Kunimaru, T., Takahashi, K., Yanagi, T., Nakano, T., Fujimaki, H., Shinjo, R., Asahara, Y., Tanimizu, M., and Dragusanu, C., 2000. JNdi-1: a neodymium isotopic reference in consistency with LaJolla neodymium. *Chem. Geol.* **168**, 279–281.

Thornton, R. C. N., 1979. Regional stratigraphic analysis of the Gidgealpa Group, southern Cooper Basin, Asutralia. *Australian Geological survey Bulletin* **49**, 140–145.

Truesdell, A. H. and Hulston, J. R., 1980. Isotopic evidence on environments of geothermal systems. In: P., F. and Fontes, J. C. Eds.), *Handbook of Environmental Isotope Geochemistry*. Elsevier, Amsterdam.

Uysal, I. T., Gasparon, M., Bolhar, R., Zhao, J.-X., Feng, Y.-X., and Jones, G., 2011a. Trace element composition of near-surface silica deposits - A powerful tool for detecting hydrothermal mineral and energy resources. *Chem. Geol.* **280**, 154–169.

Uysal, I. T. and Golding, S. D., 2003. Rare earth element fractionation in authigenic illite-smectite from Late Permian clastic rocks, Bowen Basin, Australia: implications for physico-chemical environments of fluid during illitization. *Chem. Geol.* **193**, 167–179.

Uysal, I. T., Golding, S. D., and Baublys, K., 2000. Stable isotope geochemistry of authigenic clay minerals from Late Permian coal measures, Queensland, Australia: implications for the evolution of the Bowen Basin. *Earth Planet. Sci. Lett.* **180**, 149-162.

Uysal, I. T., Golding, S. D., Bolhar, R., Zhao, J.-X., Feng, Y.-X., Baublys, K., and Greig, A., 2011b. CO_2 degassing and trapping during hydrothermal cycles related to Gondwana rifting in eastern Australia. *Geochim. Cosmochim. Acta* **75**, 5444–5466.

Veevers, J. J., 1984. *Phanerozoic earth history of Australia*. Clarendon Press, Oxford.

Veevers, J. J., Powell, C. M., and Roots, S. R., 1991. Review of seafloor spreading around Austrlia. 1. Synthesis of spreading. *Aust. J. Earth Sci.* **38**, 373–389.

Wood, S. A., 1990. The aqueous geochemistry of the rare-earth elements and yttrium: 2. Theoretical predictions of speciation in hydrothermal solutions to 350°C at saturation water vapour pressure. *Chem. Geol.* **88**, 99–125.

Woolley, A. R., 1987. Lithospheric metasomatism and the petrogenesis of the Chilwa Province of alkaline igneous rocks and carbonatites, Malawi. *Journal of African Earth Sciences* **6**, 891–898.

Yardley, B. W. D., A., B. D., Bottrell, S. H., and Diamond, L. W., 1991. Post-metamorphic gold–quartz veins from N. W. Italy: the composition and origin of the ore fluid. *Mineral. Mag.* **57**, 407–422.

Yau, Y. C., Peacor, D., Essene, E. J., Lee, J. H., and Kuo, L. C., 1987. Hydrothermal treatment of smecrite, illite, and basalt to 460°C: Comparison of natural with hydrothermally formed clay minerals. *Clays Clay Miner.* **35**, 241–250.

Ziegler, K., Sellwood, B. W., and Fallick, A. E., 1994. Radiogenic and stable isotope evidence for age and origin of authigenic illites in the Rotliegend, southern North Sea. *Clay Miner.* **29**, 555–565.

Zwingmann, H., Clauer, N., and Gaupp, R., 1999. Structure-related geochemical (REE) and isotopic (K–Ar, Rb–Sr, δ18O) characteristics of clay minerals from Rotliegend sandstone reservoirs (Permian, northern Germany). *Geochim. Cosmochim. Acta* **63**, 2805–2823.